Temperature dependence of radial breathing mode Raman frequency of single-walled carbon nanotubes

Nachiket R. Raravikar,[1] Pawel Keblinski,[1,*] Apparao M. Rao,[2] Mildred S. Dresselhaus,[3] Linda S. Schadler,[1] and Pulickel M. Ajayan[1]

[1]*Department of Materials Science and Engineering, Rensselaer Polytechnic Institute, 110, 8th Street, Troy, New York 12180*

[2]*Department of Physics and Astronomy, Clemson University, Clemson, South Carolina 29634*

[3]*Department of Physics, Massachusetts Institute of Technology, Cambridge, Massachusetts 02139*

(Received 19 July 2002; published 31 December 2002)

Recent high-temperature studies of Raman-active modes in single-walled carbon nanotube (SWNT) bundles report a softening of the radial and tangential band frequencies with increasing sample temperature. A few speculations have been proposed in the past to explain the origin of these frequency downshifts. In the present study, based on experimental data and the results of molecular dynamics simulations, we estimate the contributions from three factors that may be responsible for the observed temperature dependence of the radial breathing mode frequency $[\omega_{\mathrm{RBM}}(T)]$. These factors include thermal expansion of individual SWNTs in the radial direction, softening of the C-C (intratubular) bonds, and softening of the van der Waals intertubular interactions in SWNT bundles. Based on our analysis, we find that the first factor plays a minor role due to the very small value of the radial thermal expansion coefficient of SWNTs. On the contrary, the temperature-induced softening of the intra- and intertubular bonds contributes significantly to the temperature-dependent shift of $\omega_{\mathrm{RBM}}(T)$. For nanotubes with diameters $(d) \geqslant 1.34$ nm, the contribution due to the radial thermal expansion is $\leqslant 4\%$ over the temperature range used in this study. Interestingly, this contribution increases to $\geqslant 10\%$ in the case of nanotubes having $d \leqslant 0.89$ nm due to the relatively larger curvature of these nanotubes. The contributions from the softening of the intra- and intertubular bonds are approximately equal. These two factors together contribute a total of about ~95% and 90%, respectively, for SWNTs having $d \geqslant 1.34$ nm and $\leqslant 0.89$ nm.

DOI: 10.1103/PhysRevB.66.235424 PACS number(s): 78.66.Tr, 61.48.+c

I. INTRODUCTION

The temperature dependence of the Raman spectra of diamond, graphite, and carbon nanotubes has been reported earlier.[1–7] The shift in the Raman peak in diamond and graphite is due to a change in the elastic modulus, which can occur from changes in the interatomic distance due to thermal expansion (a volume effect) and a softening of the modulus due to the increase in temperature (temperature effect). Single-crystal graphite, or the closely related pristine highly oriented pyrolytic graphite (HOPG), has a high thermal conductivity; there is also no significant in-plane thermal expansion, and a small downshift in the Raman frequencies with increasing temperature is observed.[1] The temperature dependence of the Raman frequencies of pristine HOPG is attributed to a pure temperature effect $\sim(d\omega/dT)_v$ by Tan *et al.*[1] In fact, in case of graphite, there is a negative thermal expansion. For polycrystalline or ion-implanted graphite, the structural disorder due to the presence of defects and impurities causes a reduction in thermal conductivity. The observed downshift in the C-C bond stretching Raman frequency is large and arises due to both the volume and temperature effects. The same is true for diamond.[2] Also, in the case of carbon nanotubes, there are a few speculations about the cause of the temperature dependence of the Raman spectra, attributing this to the stretching of carbon-carbon bonds, defects, and disorder in these materials as well as to the van der Waals interactions between nanotubes in the bundles.[4,5,7] However, to the best of our knowledge, no detailed theoretical or experimental basis has been provided to support these speculations.

In graphite and carbon nanotubes, the *G*-band Raman vibrational modes (E_{2g}-derived modes) are present due to the in-plane vibrational movement of carbon atoms, which involves a combination of stretching and bending of the carbon-carbon (C-C) bonds.[8–10] The disorder-induced *D*-band Raman vibrational mode (A_{1g}), which is a highly dispersive spectral feature,[8–10] is also present in these materials due to the collective in-plane vibrational movement of atoms towards and away from the center of the hexagons formed by the covalently (sp^2) bonded carbon atoms.[11] Therefore, the *D*-band mode involves stretching and bending of C-C bonds.[11] The radial breathing mode is a unique feature in the Raman spectrum of single-walled carbon nanotubes (SWNTs) and involves a collective vibrational movement of the carbon atoms towards and away from the central axis of a SWNT.[12] The radial breathing mode oscillations are associated with a periodicity imposed on a graphene sheet by wrapping it into a finite-size (small diameter) tube. Consequently, the associated radial breathing mode (RBM) wavelength and frequency are directly related to the perimeter of the nanotube. Based on this relationship, as the diameter of the nanotube increases, the RBM frequency (ω_{RBM}) shifts to lower wave numbers.[12] For larger and, particularly, multiwalled tubes, the RBM frequency becomes very small (proportional to the inverse of tube diameter[12]) and, at the same time, the intensity of the radial breathing mode decreases and ultimately becomes undetectable by Raman spectroscopy

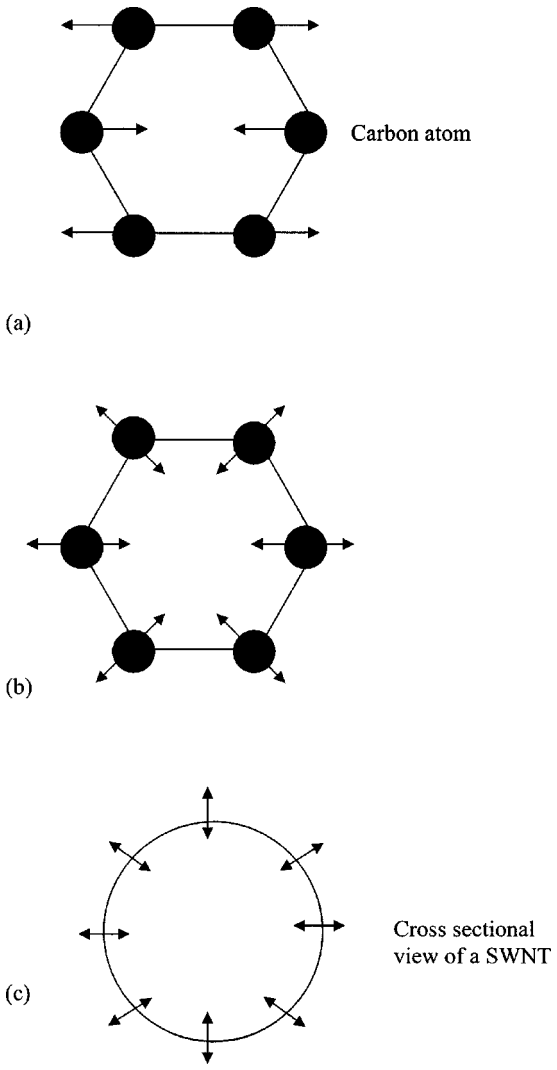

FIG. 1. Raman vibration modes in carbon nanotubes: An in-plane hexagon formed by carbon atoms is shown in (a) and (b). The arrows in all three figures show the direction of the vibrational motion of carbon atoms. (a) *G*-band (E_{2g}) mode (common to graphite). (b) *D*-band mode (common to disordered carbons and polycrystalline graphite). (c) RBM mode (unique to SWNTs, fullerenes).

measurements. In this context, a flat graphene sheet can be considered as an infinite diameter tube for which the radial breathing mode rigorously disappears. The schematics in Figs. 1(a)–1(c) show the *G*-band, *D*-band vibrational modes and the RBM's in SWNTs respectively.

The RBM frequency (ω_{RBM}) shows a strong dependence on the SWNT diameter.[13] Also, ω_{RBM} shifts to higher wave numbers when SWNTs are close packed into bundles, an effect associated with van der Waals forces, acting between nanotubes in a bundle.[13] In addition to the above-mentioned factors, the RBM frequency (ω_{RBM}) of SWNTs depends upon the strength of carbon-carbon interatomic force constants. The latter effect has typically not been explored much in the case of nanotubes.

In this paper, from a systematic analysis of the temperature dependence of ω_{RBM}, we estimate the contributions from each of these three factors in SWNT bundles. In addition to ω_{RBM}, we measure the temperature dependence of the high-frequency modes associated with stretching and bending of C-C bonds, allowing us to evaluate the temperature dependence of C-C force constants. In Sec. II, the experiments are discussed, in which we measured the temperature dependence of the Raman spectra of SWNT bundles. In Sec. III, we present the results from the molecular dynamics simulations of the thermal expansion of individual SWNTs in the radial direction. This study demonstrates that, while the corresponding coefficient of thermal expansion is very small, consistent with the results of a recent x-ray diffraction study,[14] the elastic constants exhibit significant softening with increasing temperature, due to the stretching and bending of C-C bonds. In Sec. IV, we present a quantitative analysis of the role of the various factors contributing to the temperature dependence of ω_{RBM}. Based on this analysis, we conclude that the softening of the C-C force constants in a SWNT and the van der Waals forces acting between SWNTs in bundles are predominantly responsible for the temperature-induced downshift in ω_{RBM}. Our results on the contribution from the relaxation of the van der Waals interactions between SWNTs in bundles to the temperature dependence of ω_{RBM} are consistent with those discussed earlier by Thomsen *et al.*[7]

II. EXPERIMENTAL AND RESULTS

The SWNT, approximately 94 at. % pure, synthesized by the High Pressure Carbon Monoxide (HiPco) process,[15] were purchased from Carbon Nano-technologies, Inc. The SWNTs were used for the present analysis without any further purification. A programmable hot-stage THMS 600, purchased from Linkam Scientific Instruments Ltd., was used for *in situ* heating and cooling of the SWNTs. The SWNT powder was lightly hand pressed into a pellet. The pellet was placed in a small quartz crucible, which was kept on a silver holder inside the hot stage. It was then heated and cooled in the hot stage, in flowing argon gas near atmospheric pressure, from 299 to 773 K. The samples were heated and cooled at 10 K/min, and Raman spectra were taken during heating and cooling cycles at the following temperatures: 299, 373, 473, 573, 673, and 773 K. The sample was held at each of these temperatures for 10 min while Raman spectra were taken. At each temperature the spectra were taken at four different, randomly chosen locations on the sample.

Raman spectra were collected with a Renishaw S2000 Raman spectroscope using an argon-ion laser (514 nm) at a laser power of 2.5 mW with three data accumulations and a detector data acquisition time of ~10 s. A power density of 3×10^5 W/cm^2 was used in our experiments, and the laser heating effects at these power levels were found to be minimal. The RBM peaks, the high-frequency graphitic in-plane stretching mode (*G*-band) peak, and the disorder-induced mode (*D*-band) peak were monitored. The Raman peak positions at various temperatures were determined by a peak fitting procedure that used standard software and a mixed Gaussian-Lorentzian function for the peak shape.

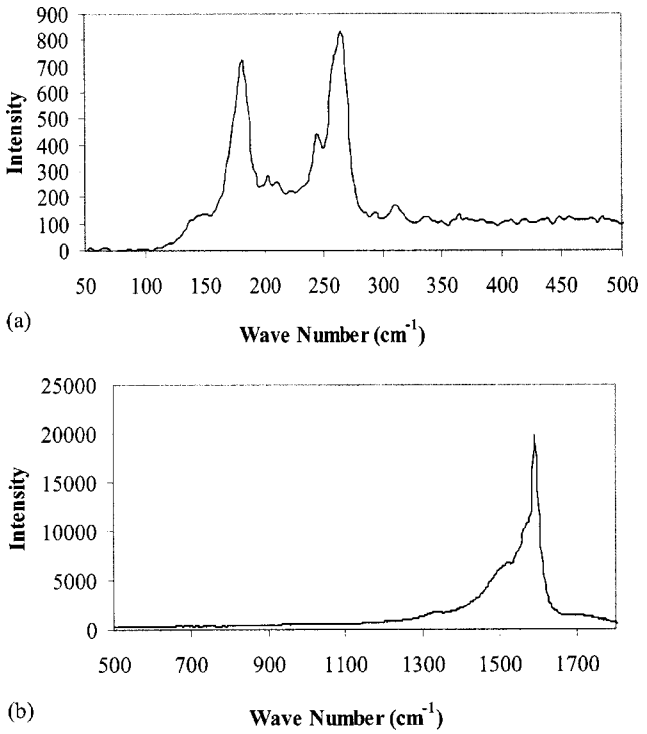

FIG. 2. Standard room-temperature Raman spectrum of as-received HiPco SWNTs taken at $E_{\text{laser}}=2.41$ eV. (a) Raman spectrum showing RBM peaks. (b) Raman spectrum showing *G*-band and *D*-band peaks.

Figures 2(a) and 2(b) show a typical Raman spectrum of our SWNT sample taken at room temperature. The two prominent peaks with a peak position of ~182 and 264 cm^{-1} in Fig. 2(a) are the two RBM peaks which have been considered in the present analysis. The two peaks from Fig. 2(b) at peak positions ~1592 and 1332 cm^{-1} belong to the *G* band (ω_G+) (Refs. 10 and 12) and *D* band, respectively, and are considered in the present analysis. Figures 3(a)–3(d) show a reversible linear shift with temperature of the two RBM frequencies, an in-plane graphitic mode (*G*–band) frequency and the disorder-induced mode (*D*-band) frequency. The two RBM peaks, with a peak position of ≈182 and 264 cm^{-1} at room temperature, which we refer to as ω_{182} and ω_{264}, correspond to the tube diameters of approximately 1.34 and 0.89 nm, respectively. These diameters are calculated using the relationship between ω_{RBM} and tube diameter for SWNT bundles.[13] Our values of $(d\omega/dT)$ of the RBM and *G*-band frequencies of SWNTs, based on the slopes of the lines in Figs. 3(a) and 3(c), are somewhat lower than the corresponding reported values.[5] This difference maybe because our HiPco-SWNT samples were not purified and were used as received, whereas the samples in Ref. 5 were purified and, hence, possibly might have undergone some chemical treatment, thereby. Thus our samples contained metallic impurities which maybe one of the factors contributing to this difference in the temperature dependence between our data and that reported in Ref. 5. However, our results were reproducible, along with a good data fit and a low scatter in the data, showing high correlation coefficients (R^2) of more than ~0.93. Therefore, these values [from Figs. 3(a)–3(c)], along

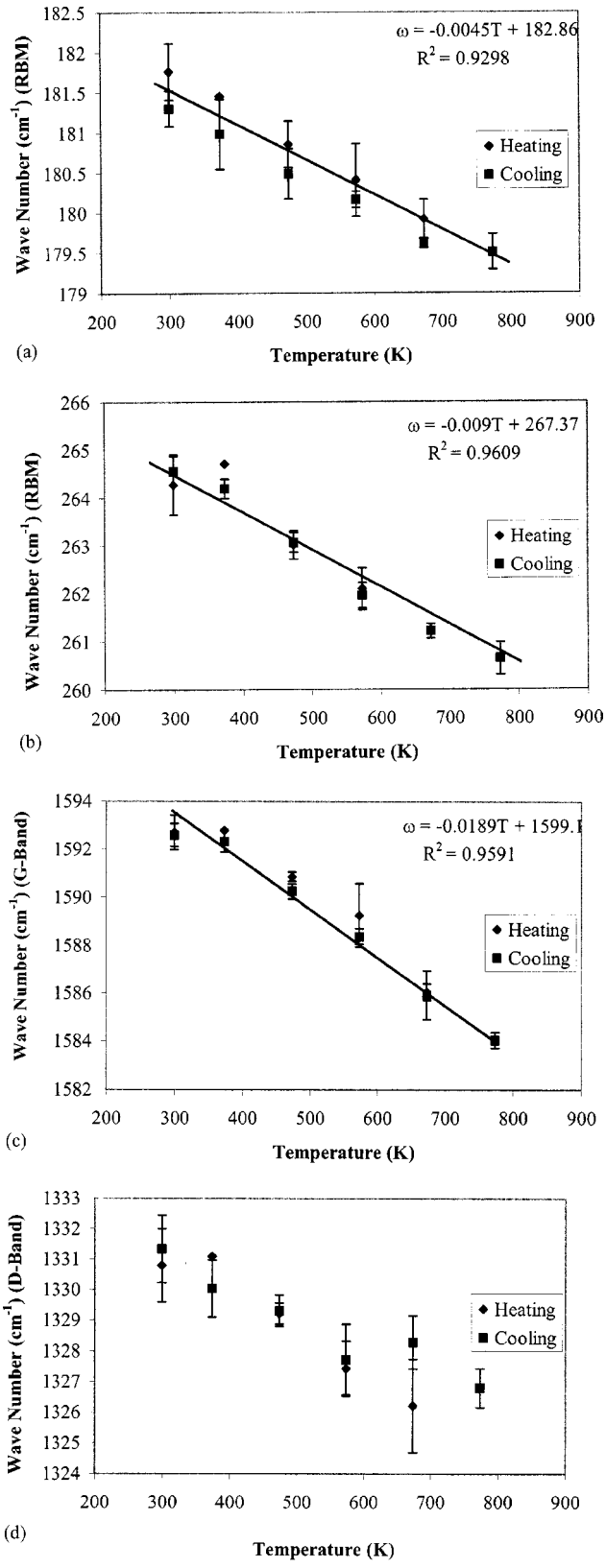

FIG. 3. Temperature dependence of Raman frequencies of SWNT plotted as wave number (cm^{-1}) vs temperature (*K*). (a) Temperature dependence of ω_{182} RBM frequency. (b) Temperature dependence of ω_{264} RBM frequency. (c) Temperature dependence of *G*-band (E_{2g}) frequency. (d) Temperature dependence of *D*-band frequency.

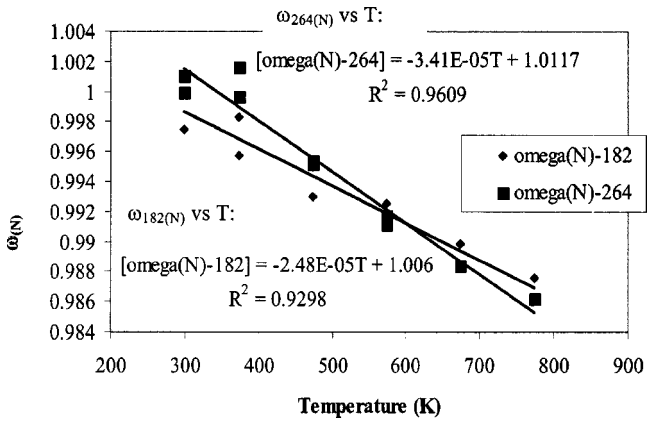

FIG. 4. $\omega_{(N)}$ vs temperature: $\omega_{(N)}$ is the normalized RBM frequency $=\omega(T)/\omega(300\ \mathrm{K})$, which is obtained from Fig. 3 by normalizing the RBM frequencies at different temperatures, with respect to the respective room-temperature RBM frequency. In the plot are shown $\omega_{182(N)}$ vs temperature and $\omega_{264(N)}$ vs temperature, which are the normalized frequencies obtained from the data in Figs. 3(a) and 3(b), respectively.

with the values obtained from the more scattered data of the *D*-band peak [Fig. 3(d)], are used in the analysis presented in Sec. IV. In the same way as described above, we also plotted the temperature dependence of the peaks at 1565 cm^{-1} (ω_G- for semi conducting tubes) (Refs. 10 and 12) and 1525 cm^{-1} (ω_G- for metallic tubes) (Refs. 10 and 12) wave numbers, and their temperature dependence in terms of $d\omega/dT$ was obtained from the slopes of the (linear) plots to be about -0.0238 and -0.0226 cm^{-1}/K, respectively. The temperature dependence of the *G*-band (ω_G+) and *D*-band modes [Figs. 3(c) and 3(d)] are used below to evaluate the softening of the C-C force constants with temperature.

In order to obtain a measure of the relative change of ω_{RBM}, we define the temperature coefficient of the RBM frequency, as $\alpha_\omega=[(d\omega/dT)/\omega(T=300\ \mathrm{K})]$. It is obtained from the slope of the plot of $\omega_{(N)}$ vs T (Fig. 4), where $\omega_{(N)}$ is the normalized RBM frequency obtained by dividing $\omega(T)$ at any temperature (Fig. 3) by the room-temperature $\omega(T=300\ \mathrm{K})$. Such a coefficient for ω_{182} can be calculated from the slope of the $\omega_{182(N)}$ vs T plot in Fig. 4 and is found to be $\alpha_{182}\cong 2.48\times10^{-5}$/K. This value represents the combined effect of all the factors responsible for the relative shift in ω_{RBM} with temperature. Similarly, the temperature coefficient for ω_{264} can be calculated from the slope of the $\omega_{264(N)}$ vs T plot in Fig. 4 and is found to be $\alpha_{264}\cong 3.41\times10^{-5}$/K. Although in the present analysis we do not take into account the effect of the tube chirality, we think that the nanotubes in the present analysis are a mixture of semiconducting and metallic tubes based on the line shape of the tangential band.[16,17]

III. MOLECULAR DYNAMICS SIMULATIONS

To provide a better understanding and explanation of the experimental data described in the previous section and to assess the role of the radial thermal expansion of SWNTs in the temperature-induced downshift of ω_{RBM}, we performed a series of molecular dynamics (MD) simulations of individual SWNTs with various diameters.

We used an empirical bond order potential due to Tersoff,[18] capable of describing both sp^2 and sp^3 carbon-carbon bonding and reproducing well the elastic properties of diamond and in-plane graphite as well as the phonon spectra of diamond. As an alternative to the Tersoff potential, we could have used the Tersoff-Brenner potential, which provides a more accurate description of the carbon-based systems.[19] However, a real shortcoming of the Tersoff potential is associated with problems involving chemical reactions, i.e., bond breaking and bond forming or systems with mixed (sp^2,sp^3) bonding. In that case, the use of the Tersoff-Brenner potential is imperative. In our modeling studies we only analyze thermomechanical properties of sp^2-bonded carbon nanotubes with no changes in their chemistry. For these types of problems, both the Tersoff and Tersoff-Brenner potentials are equally accurate. As a matter of fact, even the empirical force constant models involving just springs connecting atoms provide a faithful description of the radial breathing mode.[20] Throughout the analysis, we used a MD simulations step $\Delta t=1.7\times10^{-16}$ s, which conserves the energy to five significant figures over $10\,000\Delta t$ in a microcanonical simulation ensemble.

We first studied the thermal expansion of individual (not bundled) (5,5) and (10,10) SWNTs having diameters of 0.70 and 1.40 nm, respectively. In order to mimic the high-aspect ratio of SWNTs we used periodic boundary conditions in the axial direction. A constant-stress algorithm was applied in the axial direction, allowing the tube to expand or contract in order to maintain zero internal pressure. Furthermore, we used a velocity-rescaling algorithm to maintain constant temperature, and the data at each temperature were obtained as the averages over 100 000 MD simulations steps, proceeded by 50 000 equilibration steps. The thermal expansion data in the axial direction were simply obtained by monitoring the time-averaged length of the periodic simulation box. The data on the radial thermal expansion were obtained by monitoring the average (over all atoms and time) atomic distance from the tube center axis. As mentioned above, the diameter of (10, 10) tubes used in our MD simulations is (d) $\sim$1.40 nm. The diameter of our HiPco SWNTs, as obtained experimentally from the 182-cm^{-1} Raman peak, is d $\sim$1.34 nm. The diameter of the SWNTs used by the authors, in Ref. 14, ranges from (d)$\sim$1.36 to 1.40 nm. All of these diameters mentioned above are approximately equal. Hence we can compare the thermal expansion results of our simulations to the thermal expansion results of Ref. 14 as discussed below. This comparison is approximate because it is purely based on the similarity of diameters of nanotubes and the nanotube helicity is not considered here.

These data on the calculated axial and radial thermal expansion for (5,5) and (10,10) nanotubes are shown in Fig. 5. For both tubes, the radial thermal expansion coefficient $\alpha_{r(\mathrm{theoretical})}$ is smaller than the axial thermal expansion coefficient $\alpha_{a(\mathrm{theoretical})}$, signifying the effect of curvature on the thermal expansion properties. The calculated values of $\alpha_{r(\mathrm{theoretical})}$ are 0.35×10^{-5}/K and 0.08×10^{-5}/K for (5,5) and (10,10) SWNTs, respectively. The corresponding calcu-

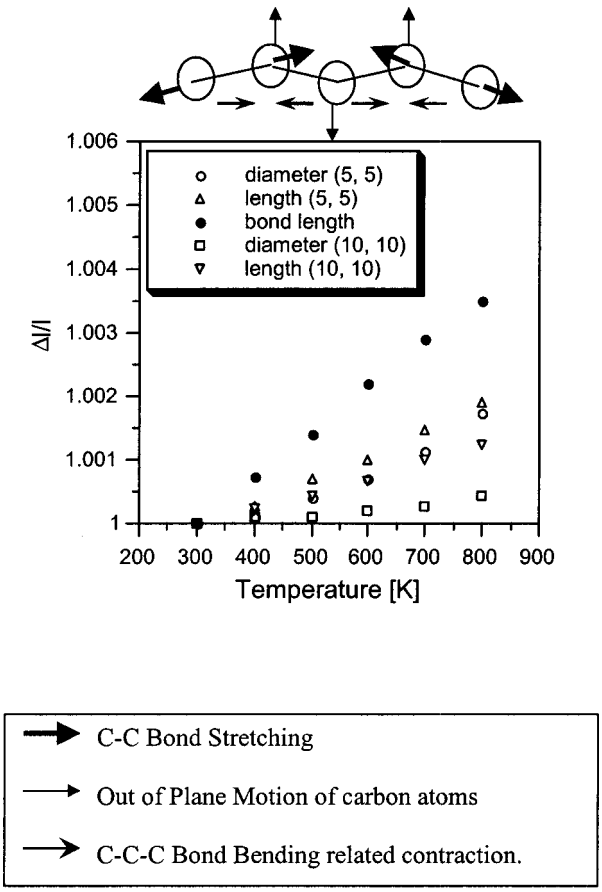

FIG. 5. Thermal expansion of the C-C bond length and of (5,5) and (10,10) SWNTs in the radial and axial directions obtained using molecular dynamics simulations. The schematic above the figure depicts how bond bending leads to the contraction of the end-to-end distance. This effect competes with the thermal expansion of the C-C bond length in determining the overall thermal expansion.

lated values for the axial thermal expansion $\alpha_{a(\text{theoretical})}$ are 0.39×10^{-5}/K and 0.24×10^{-5}/K. These results are consistent with the results from recent x-ray diffraction studies[14] of $d\sim1.34$ nm diameter SWNTs. In particular, the radial thermal expansion coefficient[14] ($\alpha_r\cong-0.15\pm0.2\times10^{-5}$/K) was observed to be slightly smaller than the axial expansion[14] ($\alpha_a\cong0\pm0.1\times10^{-5}$/K). Another effect of the curvature is the fact that the smaller diameter tubes generally are predicted to exhibit a larger α_r and α_a than larger diameter tubes. As the diameter of a nanotube becomes larger and larger, the thermal expansion coefficients become smaller and smaller and more negative, approaching α_a of graphite,[21] $\sim-1.3\times10^{-5}$/K.

The above-mentioned simulation results and the results from published x-ray diffraction experiments demonstrate that the thermal expansion of SWNTs, particularly in the radial direction, is extremely small and thus will have a minor effect on the change in radial breathing mode frequency with temperature.

At first sight these small thermal expansion coefficients might be thought to also imply that the temperature-dependent change in the C-C bond length and bond angle is also very small. In such a case, the effective C-C bond stiffness (spring constant) should also remain constant. This conjecture originates from a simple model in which the bond energy is described by a harmonic spring and a small anharmonic term.[2,22] The anharmonic term is responsible for both the thermal expansion of the bond length and the lowering of the bond stiffness.

In order to elucidate the above-described issue in our MD simulations, we monitored directly the average (over all C-C bonds and simulation times) length of the C-C bond as a function of temperature. The data in Fig. 5 show that the C-C bond length expands at a much higher rate than the radial and axial tube dimensions; the thermal expansion coefficient associated with the change in C-C bond length is $\alpha_{CC}=7.1\pm0.2\times10^{-6}$/K. This result illustrates that the anharmonicity-related bond-stretching effect is not the only one that controls the radial and axial thermal expansion behavior. This rather surprising result is associated with the fact that while, with increased temperature, the C-C bond length increases, the amplitude of the out-of-plane atomic vibrations also increases. As depicted in the schematic diagram on the top of Fig. 5, these out-of-plane vibrations tend to contract the tube. It is the competition between the bond-stretching-related expansion and the out-of-plane bond-bending-related contraction that determines the overall radial and axial thermal expansion of SWNTs (Fig. 5). It turns out that for SWNTs, as is the case for the graphite in-plane expansion, bond-stretching and bond-bending effects almost cancel each other out, leading to very low and, in fact, negative thermal expansion coefficients.

Now we turn our attention to directly simulate the radial breathing mode. To achieve this, we first equilibrated a (10, 10) nanotube (with a diameter of ~1.40 nm at constant temperature) and then suddenly increased the radial displacement of all C atoms by 0.5%. At this instant we switched to a constant-energy simulation algorithm, where atoms evolve freely according to Newton's equation of motion, with no perturbations associated with the thermostat. Then we monitored the average value of the tube radius as a function of time. Finally, to connect more directly with the experiment on the temperature dependence of the Raman spectra, we performed a Fourier transform $S(\omega_N)$ of the time-dependent tube radius.

The results obtained in the above-described procedure for several temperatures are shown in Fig. 6. The data are normalized such that the peak position at $T=300$ K (corresponding to room temperature) is normalized to unity and $\omega_N=\omega(T)/\omega(T=300\text{ K})$. Figure 6 clearly shows that the peak position shifts to lower ω_N with increasing temperature, as is also observed in the experiment. Further quantitative analysis reveals that the temperature coefficient of $d\omega_N/dT$ is of the order of -5×10^{-5}/K and negative in sign. This calculated value is much larger than the corresponding experimental value of $\alpha_{182}=-2.47\times10^{-5}$/K, but of the correct sign. The fact that the relative change in ω is significantly larger in the simulation than in experiment is not surprising considering that we use an empirical interatomic potential, which was not fitted with respect to anharmonic properties. Also, in the classical MD simulations, all of the vibrational modes (phonons) are excited at all temperatures,

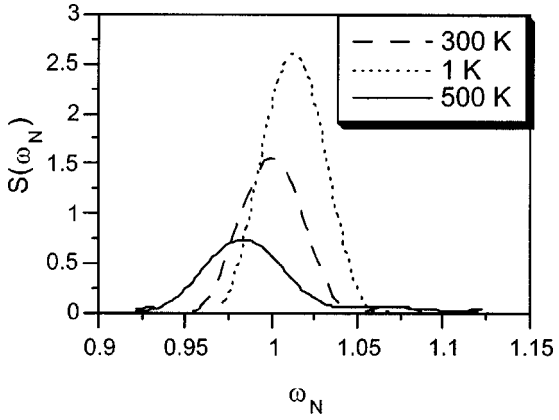

FIG. 6. Fourier transform $S(\omega_N)$ of the amplitude of the radial breathing mode of the model (10,10) carbon nanotube obtained in MD simulations for $T=1$, 300, and 500 K. The frequency is normalized such that the peak position is at $T=300$ K occurs at $\omega_N=1$.

whereas in the experiment, quantization of the energy levels freezes out high-energy (frequency) modes at low temperatures.

In view of the above-presented results, we conclude that only a small part of the temperature dependence of the frequency change of the radial breathing mode can be attributed to the very small change in the tube diameter. In turn, the only possible factor capable of explaining the change of the RBM frequency is the temperature change of the C-C bond force constant (tube bundling effects are not present in our simulations, since we only consider individual tubes). We will discuss this issue in detail in the next section.

In order to illustrate the temperature effect of the force constant change more directly, we present in Fig. 7 the temperature dependence of Young's modulus calculated from the stress-strain curves obtained in the MD simulations of (10, 10) tubes. Also, analogous to the previous analysis, we normalize the calculated Young's modulus by its corresponding value at $T=300$ K. The temperature-dependent relaxation of the elastic modulus of various materials has been demonstrated earlier, where it was shown that the modulus decreases linearly with increasing temperature.[23–25] Figure 7

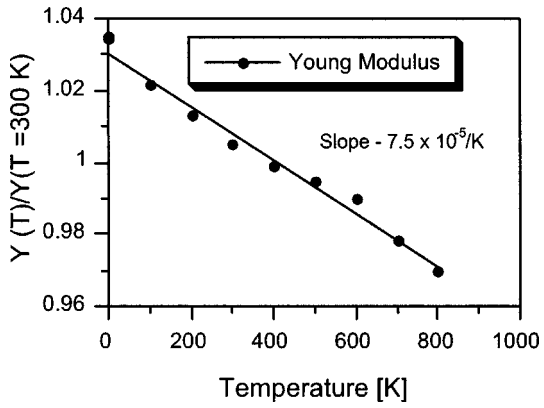

FIG. 7. Young's modulus normalized by its value at $T=300$ K, for the (10, 10) carbon nanotube.

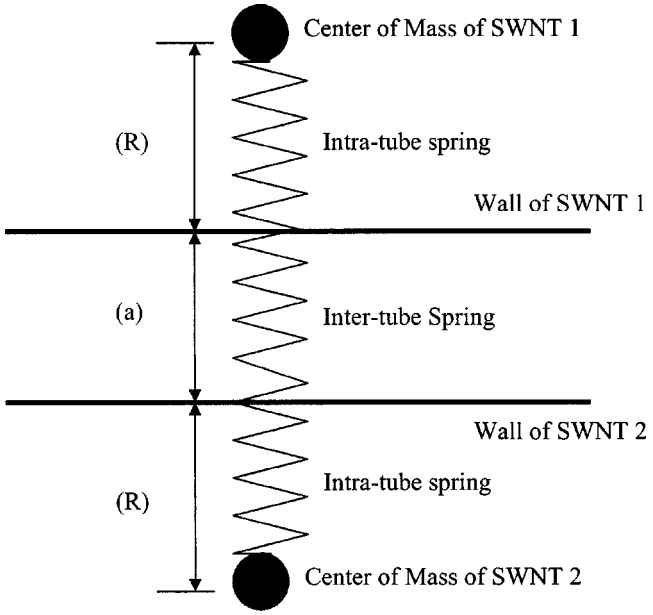

FIG. 8. Spring model for adjacent tubes inside a SWNT bundle: The intertube spring is a function of the weak van der Waals interactions between two SWNTs. The intratube spring is a function of: (1) mainly, the interatomic (carbon-carbon) bonds of a SWNT and (2) the diameter of the SWNT ($K_{\text{intraspring}}>K_{\text{interspring}}$). ($R$) is the radius of the SWNT, measured as the distance between the center of mass of the tube and the tube wall; (a) is the distance between the tube walls.

illustrates that the calculated (normalized) Young's modulus of nanotubes decreases with increasing temperature; the associated temperature coefficient $[dY(T)/dT]/Y(T=300\ \text{K})$ is equal to $\sim -7\times10^{-5}$/K, which is of similar order to the simulated temperature coefficient of ω_{RBM}. This provides further evidence that the temperature-dependent softening of the C-C bond stiffness and the related elastic properties play an important role in the temperature change of ω_{RBM}. In contrast, the diameter change associated with the thermal expansion of the lattice plays only a secondary role.

IV. THEORETICAL ANALYSIS AND DISCUSSION

Having discussed the relative temperature-dependent effects of the thermal expansion of the nanotube diameter and of the relaxation of the interatomic force constants on the temperature-dependent shift of the ω_{RBM} of SWNTs, we now attempt to obtain a theoretical understanding and quantification of the relative contributions of these effects.

We start with a formulation of a model representing both the strong covalent C-C bonds within each tube and the weak van der Waals forces acting between the tubes. The weak van der Waals forces lead to a bundling of the SWNTs into close-packed structures that form a triangular lattice.[5,14,15] The model, as depicted in Fig. 8, involves an effective intratubular spring constant k_{intra} representing the net force exerted on a carbon atom from all the other atoms in the SWNT. The model also involves an effective intertubular spring constant k_{inter} representing the interactions between tubes in the bundle.

As depicted in the schematic in Fig. 8, the forces from these two springs both contribute to the RBM frequency. Thus ω_{RBM} can be expressed in terms of the frequencies of these two springs as

$$\omega_{\mathrm{RBM}}=\sqrt{\omega_{\mathrm{intra}}^2+\omega_{\mathrm{inter}}^2}. \tag{1}$$

Consequently, the temperature dependence of ω_{RBM} can be expressed in terms of the temperature dependence of the frequencies of these two springs, as follows:

$$\frac{d\omega_{\mathrm{RBM}}}{dT}=\frac{\partial\omega_{\mathrm{RBM}}}{\partial\omega_{\mathrm{intra}}}\frac{d\omega_{\mathrm{intra}}}{dT}+\frac{\partial\omega_{\mathrm{RBM}}}{\partial\omega_{\mathrm{inter}}}\frac{d\omega_{\mathrm{inter}}}{dT}. \tag{2}$$

Finding partial derivatives with the use of Eq. (1) yields

$$\frac{d\omega_{\mathrm{RBM}}}{dT}=\frac{\omega_{\mathrm{intra}}}{\omega_{\mathrm{RBM}}}\frac{d\omega_{\mathrm{intra}}}{dT}+\frac{\omega_{\mathrm{inter}}}{\omega_{\mathrm{RBM}}}\frac{d\omega_{\mathrm{inter}}}{dT}. \tag{3}$$

In order to illustrate the magnitude of ω_{intra} and ω_{inter}, we use the experimental data[13] for $d\sim1.34$ nm tubes, stating that the $\omega_{\mathrm{RBM}}=182\ \mathrm{cm}^{-1}$ involving tubes in a bundle is 14 wave numbers higher than the RBM frequency of separated tubes, $\omega_{\mathrm{intra}}=168\ \mathrm{cm}^{-1}$. Using Eq. (1) one gets $\omega_{\mathrm{inter}}\approx70\ \mathrm{cm}^{-1}$.

First, let us discuss the temperature dependence $[d\omega_{\mathrm{intra}}/dT]$. Since ω_{intra} represents the frequency of vibration of a cylinder in the RBM mode, it really depends on the stiffness of the C-C bonds and on the tube diameter d. A simple vibrational analysis yields[22]

$$\omega_{\mathrm{intra}}=A\frac{\sqrt{k_{\mathrm{CC}}}}{d}, \tag{4}$$

where k_{CC} is the spring constant associated with the C-C bond and is a function of the in-plane C-C bond-stretching force constant (K) and the bond-bending force constant (H), and A is a proportionality constant. Therefore, the temperature dependence of ω_{intra} will be a function of the temperature dependence of the interatomic force constants and the change in tube diameter due to thermal expansion. It can be quantified in a form analogous to Eq. (2) as

$$\frac{d\omega_{\mathrm{intra}}}{dT}=\frac{\partial\omega_{\mathrm{intra}}}{\partial d}\frac{dd}{dT}+\frac{\partial\omega_{\mathrm{intra}}}{\partial k_{\mathrm{CC}}}\frac{dk_{\mathrm{CC}}}{dT}. \tag{5}$$

The first term in the above equation is related to the thermal expansion of a SWNT in the radial direction and, by combining Eqs. (4) and (5), gives

$$\frac{\partial\omega_{\mathrm{intra}}}{\partial d}\frac{dd}{dT}=-\omega_{\mathrm{intra}}\alpha_r, \tag{6}$$

where $\alpha_r=1/d\ dd/dT$ is the radial thermal expansion coefficient. Inserting Eq. (6) into Eq. (5) and then Eq. (5) into Eqs. (2) and (3), the contribution to $d\omega_{\mathrm{RBM}}/dT$ [see Eq. (2)] from the nanotube diameter change can be expressed as

$$\frac{\partial\omega_{\mathrm{RBM}}}{\partial\omega_{\mathrm{intra}}}\frac{\partial\omega_{\mathrm{intra}}}{\partial d}\frac{dd}{dT}=\frac{\omega_{\mathrm{intra}}}{\omega_{\mathrm{RBM}}}\omega_{\mathrm{intra}}\alpha_r. \tag{7}$$

The contribution described by the above equation is small due to the small value of the $|\alpha_r|\leqslant2\times10^{-6}$/K. For example, in the case of ω_{182}, the contribution from the change in the tube diameter (obtained by using $\omega_{\mathrm{RBM}}=182\ \mathrm{cm}^{-1}$, $\omega_{\mathrm{intra}}=168\ \mathrm{cm}^{-1}$, $\alpha_r\sim1\times10^{-6}$/K from the x-ray diffraction studies[14]) is at the most ~4% of the total observed change $d\omega_{\mathrm{RBM}}/dT$ when the value obtained using Eq. (7) is compared with the slope of the line in Fig. 3(a).

In order to evaluate the effect of the temperature dependence of $d\omega_{\mathrm{RBM}}/dT$ associated with the intratubular interactions, the second term in Eq. (5) needs to be evaluated. We first rewrite the formula given by Eq. (4) in terms of the elastic moduli and the mass density of the graphite reference material, given by[26]

$$\omega_{\mathrm{intra}}=\frac{1}{\pi cd\sqrt{\rho}}\sqrt{\frac{C_{11}^2-C_{12}^2}{C_{11}}}, \tag{8}$$

where ρ is the density of graphite, C_{11} and C_{12} are the in-plane elastic moduli, and c is the speed of light in cm/s, which converts the Raman wave number expressed in cm^{-1} units to the frequency expressed in s^{-1} units. C_{11} and C_{12} are related to the C-C bond-stretching force constant (K) and bond-bending force constant (H) through the following relationships, originally given for graphite[27] and used by us for the SWNT as a reasonable approximation:

$$C_{11}=Kr_0^2N_0\frac{K+18H}{2K+12H},\quad C_{12}=Kr_0^2N_0\frac{K-6H}{2K+12H}. \tag{9}$$

In the above equations, r_0 is the interatomic C-C distance (~1.42 Å),[27] and N_0 is the atomic number density ($N_0\sim1.14\times10^{23}$ atoms/cm^3).[27] The in-plane force constants K and H can be obtained from the G-band (~1592 cm^{-1}) and D-band (~1332 cm^{-1}) frequencies according to the relationships[11]

$$f(D\ \text{band})=\sqrt{\frac{3K}{m_{\mathrm{C}}}},\quad f(G\ \text{band})=\sqrt{\frac{3K+18H}{m_{\mathrm{C}}}}. \tag{10}$$

In the above relationships, m_{C} is the mass of a carbon atom, f is the frequency of vibration$=2\pi c\omega$, where ω is the wave number measured from the Raman spectrum, and c is the speed of light, which, as discussed above, converts the ω into cm^{-1} units to f into s^{-1} units. It is known that the D band is highly dispersive; its frequency changes when the laser energy changes. However, since the laser energy is 2.41 eV throughout our experiment, the D-band shift measured in this work does not take dispersion into account and can be related only to the temperature-dependent relaxation of the spring constants at constant $E_{\mathrm{laser}}\geqslant2.41$ eV. We expect the temperature dependence of the dispersion $\partial^2\omega/\partial E_{\mathrm{laser}}\partial T$ to be a second-order effect.

Now we can express the contribution to $d\omega_{\mathrm{RBM}}/dT$ due to the changes in C-C force constants associated with the second term in Eq. (5), in terms of (dK/dT) and (dH/dT) obtained from the measured D- and G-band Raman peaks and Eq. (9) (see Fig. 9). Using familiar derivative equalities,

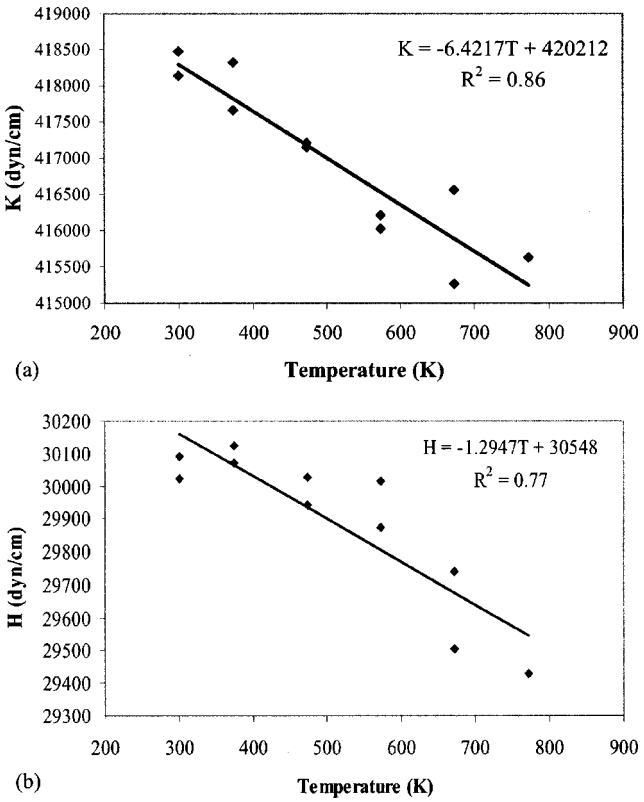

FIG. 9. Temperature dependence of interatomic force constants: Each data point is an average of the data points taken at each temperature, while heating and cooling the sample from 299 to 773 K. These data points are derived from those in Figs. 3(c) and 3(d) and using Eq. (10). (a) Temperature dependence of bond-stretching force constant (K). (b) Temperature dependence of bond-bending force constant (H).

the contribution of the C-C force constants to the $d\omega_{\mathrm{RBM}}/dT$ given by Eq. (3) is evaluated as

$$\frac{\partial \omega_{\mathrm{RBM}}}{\partial \omega_{\mathrm{intra}}}\left[\frac{\partial \omega_{\mathrm{intra}}(K,H)}{\partial K}\frac{dK}{dT}+\frac{\partial_{\mathrm{intra}}(K,H)}{\partial H}\frac{dH}{dT}\right], \qquad (11)$$

where the values of K and H, as well as (dK/dT) and (dH/dT), can be obtained from Figs. 9(a) and 9(b), and the partial derivatives can be obtained analytically, in turn, from Eqs. (1), (8), and (9).

In contrast to the contribution from the diameter change due to thermal expansion, the contribution arising from the softening of the C-C bonds is significant due to the relatively large changes in the K and H force constants with temperature. Equation (11), applied for ω_{182}, leads to the evaluation of the contribution from the change in the intratubular force constant, equal to ~50% of the total observed change $d\omega_{\mathrm{RBM}}/dT$.

Now we discuss the contribution from the temperature dependence of the frequency, ω_{inter}, due to softening of the intertube spring and corresponding to the second term in Eq. (2). An estimate of this contribution can be obtained for the relationship between the thermal expansion of SWNT bundles and the temperature dependence of ω_{inter}, since both effects, in this case, are controlled by the anharmonicity of the intertubular interactions.

For isotropic solids, the above-discussed relationship can be written in the following form[2]

$$\omega_{\mathrm{inter}}(T)=\omega_{\mathrm{inter}}(T_R)\exp\left(-3\gamma\int_{T_R}^{T}\alpha(T)dT\right), \qquad (12)$$

where γ is the Grüneisen constant and T_R is room temperature. The Grüneisen constant is related to the thermal expansion coefficient via[22,28]

$$\gamma=\frac{\alpha V}{\chi C_V}, \qquad (13)$$

where V is the molar volume, χ is the bulk compressibility, and C_V is the heat capacity.

SWNT bundles exhibit a large thermal expansion, controlled by the weak intertube forces, but only in the directions perpendicular to the tube axis. Therefore, Eqs. (12) and (13) are not strictly applicable, since they were derived for isotropic solids. However, they still provide a good estimate for the behavior of SWNT bundles.

Considering that the argument of the exponent in Eq. (12) is much smaller than unity, by first expanding the exponent and then taking the temperature derivative of ω_{inter}, one obtains

$$\frac{d\omega_{\mathrm{inter}}(T)}{dT}=-3\omega_{\mathrm{inter}}(T_R)\gamma\alpha. \qquad (14)$$

Using Eq. (13), with the experimental value of the coefficient of thermal expansion of SWNT bundles,[14] $\alpha=0.75\times10^{-5}$/K, and their bulk compressibility,[29] $\chi\sim0.0024\ \mathrm{GPa}^{-1}$, the Grüneisen constant can be calculated to be equal to ~3.6, where we take V as the molar volume for ~1.34 nm tubes, $V=(12\ \mathrm{g})/(1.33\ \mathrm{g/cm^3})\cong9\ \mathrm{cm^3}$, and the heat capacity, $C_v\sim7.8$ J/mol K, at room temperature.[30]

Finally, using Eq. (14), the temperature dependence of ω_{inter} for ω_{182} can be evaluated. The value so obtained, along with $\omega_{\mathrm{inter}}=70\ \mathrm{cm}^{-1}$ inserted into Eq. (3), is approximately equal to the contribution due to the relaxation of the intratubular force constants. These two contributions, that is, the relaxation of the intra- and intertubular forces, together result in ~95% of the total observed change $d\omega_{\mathrm{RBM}}/dT$. It should be noted that these individual contributions are approximate values, obtained using several assumptions. The smaller diameter tubes, such as $d\sim0.89$ nm tubes, have larger curvature than the $d\sim1.34$ nm tubes. Hence a direct application of equations, such as Eqs. (9) and (10), for solving Eq. (11), may be less accurate in predicting the contribution due to the relaxation of the intratubular force constants for smaller diameter tubes. Also, our analysis, to a first-degree approximation, is mostly diameter dependent, although it will be interesting to take into account the effect of the helicity of the nanotubes on the intratubular and intertubular contributions. We predict that these contributions may be approximately independent of the helicity of the nanotubes, because our equations do not involve parameters which describe the he-

licity. Nevertheless, our estimate, as of now, shows that the dominant contribution to the shift in the RBM frequency originates from the softening of the intra- and intertubular forces, and that the contributions from each of these two factors are approximately equal.

V. CONCLUSIONS

Based on our estimates for each of the three contributing factors to the temperature dependence of $\omega_{\mathrm{RBM}}(T)$, we find that the dominant contributions result from temperature-induced softening of the intratubular C-C bond strength and from the SWNT intertubular (van der Waals) interactions. Furthermore, these factors contribute approximately equally to the total change of $\omega_{\mathrm{RBM}}(T)$ with temperature. In contrast, the small value for the thermal expansion of SWNTs leads to a smaller contribution to the temperature-dependent change of $\omega_{\mathrm{RBM}}(T)$. As demonstrated by the results of the molecular dynamics simulations, this small value of the thermal expansion originates from the almost exact cancellation of the effect of the C-C bond length expansion and bond-bending-related contraction.

The temperature coefficient of the normalized RBM frequency, $\omega_{264}(T)/\omega_{264}(300\ \mathrm{K})$, of tubes with $d \sim 0.89$ nm is about 30% greater than that observed for tubes with $d \sim 1.34$ nm (Fig. 4). One origin for this increase is that the smaller diameter tubes exhibit a larger radial thermal expansion associated with relatively larger curvature. For example, based on our molecular dynamics simulation results (Fig. 5), we estimate that, while the effects of the softening of intra- and intertubular interactions still dominate, the contribution from the radial thermal expansion to the temperature dependence of $\omega_{\mathrm{RBM}}(T)$ for the (5, 5) SWNT is increased to approximately 10%. Importantly, regardless of the tube diameter, the contributions from the softening of the intra- and intertubular interactions are still dominant and the calculations suggest that they contribute approximately equally to the temperature dependence of $\omega_{\mathrm{RBM}}(T)$ for typical SWNT diameters.

ACKNOWLEDGMENTS

The authors thank Dr. Robert Vajtai for useful discussions and the National Science Foundation funded Nanoscale Science and Engineering Center (NSEC) for directed assembly of nanostructures at RPI. P.K. was also supported by the NSF Grant No. DMR 134725. A.M.R. acknowledges support for this work from a grant through NASA Ames Research Center and ERC-NSF Award No. EEC-9731680. M.S.D. acknowledges support from NSF Grant No. DMR 01-16042.

*Author to whom all correspondence should be addressed. Present address: Room 142, Materials Research Center, Department of Materials Science and Engineering, Rensselaer Polytechnic Institute, 110, 8th Street, Troy, NY 12180. Electronic address: keblip@rpi.edu

[1] P. Tan, Y. Deng, Q. Zhao, and W. Cheng, Appl. Phys. Lett. **74**, 1818 (1999).
[2] E. S. Zouboulis and M. Grimsditch, Phys. Rev. B **43**, 12 490 (1991).
[3] P. V. Houng, R. Cavagnat, P. M. Ajayan, and O. Stephan, Phys. Rev. B **51**, 10 048 (1995).
[4] F. Huang, K. T. Yue, P. Tan, S.-L. Zhang, Z. Shi, X. Zhou, and Z. Gu, J. Appl. Phys. **84**, 4022 (1998).
[5] H. D. Li, K. T. Yue, Z. L. Lian, Y. Zhan, L. X. Zhou, S. L. Zhang, Z. J. Shi, Z. N. Gu, B. B. Liu, R. S. Yang, H. B. Yang, G. T. Zou, Y. Zhang, and S. Iijima, Appl. Phys. Lett. **76**, 2053 (2000).
[6] E. D. Obraztsova, V. Yu. Yurov, V. M. Shevluga, R. E. Baranovsky, V. A. Nalimova, V. L. Kuznetsov, and V. I. Zaikovskii, Nanostruct. Mater. **11**, 295 (1999).
[7] C. Thomsen, S. Reich, A. R. Goni, H. Jantoljak, P. M. Rafailov, I. Loa, K. Syassen, C. Journet, and P. Bernier, Phys. Status Solidi B **215**, 435 (1999).
[8] C. Thomsen and S. Reich, Phys. Rev. Lett. **85**, 5214 (2000).
[9] R. Saito, A. Jorio, A. G. Souza Filho, G. Dresselhaus, M. S. Dresselhaus, and M. A. Pimenta, Phys. Rev. Lett. **88**, 027401 (2002).
[10] M. S. Dresselhaus, G. Dresselhaus, A. Jorio, A. G. Souza Filho, and R. Saito, Carbon **40**, 2043 (2002).
[11] F. Tuinstra and J. L. Koenig, J. Chem. Phys. **53**, 1126 (1970).
[12] M. S. Dresselhaus and P. C. Eklund, Adv. Phys. **49**, 705 (2000).
[13] A. M. Rao, J. Chen, E. Richter, U. Schlecht, P. C. Eklund, R. C. Haddon, U. D. Venkateswaran, Y.-K. Kwon, and D. Tomànek, Phys. Rev. Lett. **86**, 3895 (2001).
[14] Y. Maniwa, R. Fujiwara, H. Kira, H. Tou, H. Kataura, S. Suzuki, Y. Achiba, E. Nishibori, M. Takata, M. Sakata, A. Fujiwara, and H. Suematsu, Phys. Rev. B **64**, 241402(R) (2001).
[15] M. J. Bronikowski, P. A. Willis, D. T. Colbert, K. A. Smith, and R. E. Smalley, J. Vac. Sci. Technol. A **19**, 1800 (2001).
[16] M. A. Pimenta, A. Marucci, S. A. Empedocles, M. G. Bawendi, E. B. Hanlon, A. M. Rao, P. C. Eklund, R. E. Smalley, G. Dresselhaus, and M. S. Dresselhaus, Phys. Rev. B **58**, R16 016 (1998).
[17] H. Kataura, Y. Kumazawa, Y. Maniwa, I. Umezu, S. Suzuki, Y. Ohtsuka, and Y. Achiba, Synth. Met. **103**, 2555 (1999).
[18] J. Tersoff, Phys. Rev. Lett. **61**, 2879 (1988).
[19] D. W. Brenner, Phys. Rev. B **42**, 9458 (1990).
[20] V. P. Sokhan, D. Nicholson, and N. Quirke, J. Chem. Phys. **113**, 2007 (2000).
[21] A. C. Bailey and B. Yates, J. Appl. Phys. **41**, 5088 (1970).
[22] N. W. Ashcroft and N. D. Mermin, *Solid State Physics* (Harcourt College, Orlando, 1976).
[23] R. Ramji Rao and A. Ramanand, Phys. Status Solidi B **87**, 751 (1978).
[24] R. B. McLellan and T. Ishikawa, J. Phys. Chem. Solids **48**, 603 (1987).
[25] A. Vijay and T. S. Verma, Physica B **291**, 373 (2000).
[26] G. D. Mahan, Phys. Rev. B **65**, 235402 (2002).
[27] B. T. Kelly, *Physics of Graphite* (Applied Science, London, 1981).
[28] D. F. Gibbons, Phys. Rev. **112**, 136 (1958).
[29] J. Tang, L.-C. Qin, T. Sasaki, M. Yudasaka, A. Matsushita, and S. Ijima, Phys. Rev. Lett. **85**, 1887 (2000).
[30] J. Hone, B. Batlogg, Z. Benes, A. T. Johnson, and J. E. Fischer, Science **289**, 1730 (2000).